DOI: 10.17344/acsi.2019.5066 *Acta Chim. Slov.* **2019,** *66,* 490–500

Scientific paper

Synthesis, X-Ray Structure Determination and Related Physical Properties of Thiazolidinone Derivative by DFT Quantum Chemical Method

Youcef Megrouss,[1,*] Fayssal Triki Baara,[2] Nourdine Boukabcha,[1] Abdelkader Chouaih,[1] Antonis Hatzidimitriou,[3] Ayada Djafri,[2] Fodil Hamzaoui[4]

[1] *LTPS Laboratory, University Abdelhamid Ibn Badis - Mostaganem, 27000 Mostaganem, Algeria*

[2] *Laboratory of Applied Organic Synthesis (LSOA), Department of Chemistry, Faculty of Sciences, University of Oran-1 Ahmed Ben Bella, 31000 Oran, Algeria*

[3] *Department of General and Inorganic Chemistry, Faculty of Chemistry, Aristotle University of Thessaloniki, GR-54124 Thessaloniki, Greece*

[4] *LPFM Académie de Montpellier, France*

** Corresponding author: E-mail: youmeg@hotmail.fr*

Received: 02-20-2019

Abstract

In this paper we report the synthesis and characterization of the (*Z*)-3-*N*-(ethyl)-2-*N*'-((3-methoxyphenyl)imino)thiazolidine-4-one by means of FT-IR, ^{1}H and ^{13}C NMR and by single crystal X-ray diffraction. The experimental determination of the crystal structure of the compound has been achieved using X-ray diffraction data. The important characteristic of the structure is the existence of a dihedral angle formed by the benzene and thiazolidinone rings being equal to 86.0° indicating an absence of π–π stacking as well as that the structure is non planar. In the crystal, the molecules are linked by C–H···O and C–H···N hydrogen bonds, these bonds being responsible for the three-dimensional molecular structure packing. In order to compare the experimental results with those of the theoretical calculation, quantum chemical DFT calculations were carried out using B3LYP/6-311G(d,p) basis set. In this context, the molecular electrostatic potential around the molecule and HOMO–LUMO energy levels were also computed. The dipole moment orientations were determined in order to understand the nature of inter- and intramolecular charge transfer. Finally, the stability of the title compound was confirmed throughout the calculation of the chemical reactivity descriptors.

Keywords: X-ray diffraction; single crystal; DFT calculations; spectroscopy; FT-IR; ^{1}H and ^{13}C NMR.

1. Introduction

Heterocyclic compounds are the major family of organic compounds; in medicinal chemistry thiazole derivatives are of great importance for their chemical and pharmacological properties, consequently thiazole derivatives have an extended range of pharmacological applications. Over the years, interesting biological activities were combined with thiazole derivatives.[1–2] These materials are extremely necessary with wide range of synthetic, pharmaceutical and industrial applications and are famous for their biological activities.[3,4] Recently, in drug development the application of thiazoles was required for the treatment of allergies,[5] hypertension,[6] inflammation,[7] schizophrenia,[8] bacterial[9] and HIV infections,[10] as hypnotics[11] and more recently for pain treatment,[12] as fibrinogen receptor antagonists with antithrombotic activity.[13] In addition, thiazolidinones and thiazoles present a very powerful activity as anti mycobacterium in tuberculosis.[14] In this context, we have tried to realize the synthesis of the title compound, to characterize and perform its structural analysis as well as the theoretical density functional theory (DFT) calculations. In this work we present the synthesis, single crystal structure, IR and NMR spectroscopic characterizations as well as DFT calculations of this new thiazole derivative compound, namely the (*Z*)-3-*N*-(ethyl)-2-*N*'-((3-methoxyphenyl)imi-

no)thiazolidine-4-one. Furthermore, theoretical vibrational frequencies and ^{1}H and ^{13}C NMR chemical shifts were calculated and compared to the experimental values. Additional parameters as molecular orbitals and chemical reactivity descriptors are evaluated in order to confirm the stability of the title compound. Finally, the molecular electrostatic potential was computed to determine electrophilic and nucleophilic regions of the title molecule.

2. Experimental

2. 1. Synthesis and Crystallization

An equimolar solution of *N*-ethyl-3-*N*'-(3-methoxyphenyl)thiourea and ethyl bromoacetate in absolute ethanol in the presence of sodium acetate was refluxed for 6 h. The solvent was removed by vacuum distillation and the residue was isolated, washed with cold water, filtered, dried and crystallized from ethanol to yield (*Z*)-3-*N*-(ethyl)-2-*N*'-((3-methoxyphenyl)imino)thiazolidin-4-one as presented in the scheme 1.

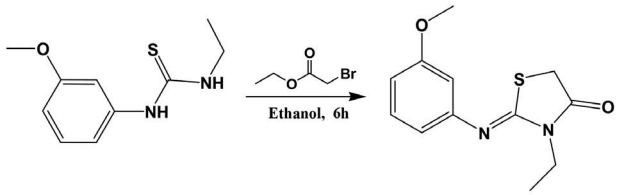

Scheme 1. Reaction sequence for the title compound synthesis.

2. 2. Spectral Data Measurements

Infrared (IR) spectrum of the molecule (*Z*)-3-*N*-(ethyl)-2-*N*'-((3-methoxyphenyl)imino)thiazolidine-4-one was recorded in the range 500–4000cm^{-1} on a Nicolet FT-IR 6700 spectrometer using sample prepared as KBr pellets. ^{1}H NMR (500 MHz) and ^{13}C NMR (125 MHz) spectra of the molecule using $CDCl_3$ as the solvent were recorded on Bruker AC250 spectrometer at 298 K.

2. 3. X-Ray Data Collection and Processing

A transparent-yellowish parallelepiped crystal was selected and separated from the mother liquor, immediately cooled to 130 K and mounted on a Bruker Kappa APEX 2 diffractometer, equipped with a Triumph monochromator using MoKa radiation. The crystal presented no decay during the data collection. The frames collected (running ϕ and ω scans) were integrated with the Bruker SAINT Software package,[15] using a narrow-frame algorithm. Data were corrected using the SADABS program.[16] The structure was solved by the SUPERFLIP package.[17] Crystals program package version 14.40[18] has been used for the refinement and all the rest subsequent calculations through full-matrix least-squares on F^2. All non-hydrogen atoms have been refined anisotropically. Hydrogen atoms were found at their expected positions and refined using proper riding constraints to the pivot atoms. Molecular illustrations were made through the MoPro-viewer crystallographic program.[19] Crystallographic and experimental details are summarized in Table 1.

Table 1. Crystallographic and experimental details.

Crystal data	
Chemical formula	$C_{12}H_{14}N_2O_2S$
M_r	250.32
Crystal system	Monoclinic
Space group	*C*2/*c*
a (Å)	23.7067 (19)
b (Å)	6.8884 (6)
c (Å)	15.7244 (12)
β (°)	111.6504 (17)
V (Å^3)	2386.66 (18)
Z	8
μ (mm^{-1})	0.26
Crystal size (mm)	0.31 × 0.28 × 0.19
Diffractometer	Bruker Kappa Apex2
Absorption correction	Numerical Analytical Absorption (De Meulenaer & Tompa, 1965)
T_{min}, T_{max}	0.93, 0.95
Radiation type, λ (Å)	Mo *K*α, 0.71073
Temperature (K)	130
Measured	17268
Independent	
Observed [$I > 2.0\sigma(I)$]	3006
2843	
R_{int}	0.015
$R[F^2 > 2\sigma(F^2)]$	0.029
$wR(F^2)$	0.066
S	1.00
No. of reflections	2843
No. of parameters	154
$\Delta\rho_{max}$, $\Delta\rho_{min}$ (e Å^{-3})	0.33, 0.21

3. DFT Calculations

In this theoretical study, the hybrid functional B3LYP with the 6-311G (d, p)[20] basis set were used in all calculations by using the Gaussian 09 program,[21] the X-ray structure was used as starting geometry to optimize a molecular structure of the investigation compound. Vibrational frequencies were calculated and the Gauss-view molecular visualization program[22] and VEDA software[23] were used for the assignment. Additionally, ^{1}H and ^{13}C NMR chemical shifts were calculated using the same level of theory. The theoretical calculation also allowed us to compute the energy values of the highest occupied molecular orbital (HOMO) and lowest unoccupied molecular orbital (LUMO). Furthermore, the molecular electrostatic

potential was calculated with B3LYP/6-311G(d, p) to highlight the electrophilic and nucleophulic attack sites.

4. Results and Discussion

4. 1. Structure Description

The molecular geometry of the title compound is defined by the presence of two fragments, methoxyphenyl and thiazolidine rings forming a dihedral angle of 86°. Detailed results containing atomic positions and thermal parameters are given in the CIF file. Selected bond lengths, bond and torsion angles for all atoms by X-ray diffraction and theoretical calculations are listed in Tables 2, 3 and 4, respectively. An ORTEPIII diagram[24] of the title compound showing the X-ray structure with thermal ellipsoids of the different atoms and the theoretical structure are given in Figure 1. In our study we employed full geometry optimization for the molecule without symmetry constraint. The results of our calculations showed that S1–C5, S1–C1, C1–N1, N1–C2, N1–C4, C6–N2 and O 2–C8 bonds exhibit single bond characteristics, while C4–O2 (1.23 Å) and N2–C1 (1.26 Å) bonds show typical double bond characteristics.[25] The amine N2 atom exhibits a geometry that is typical for an sp^2 rather than an sp^3 atom hybridisation. In addition, the difference in the thiazole ring bonds between theoretical calculation and experimental values does not exceed 0.13 Å. Bond angles C6–N2–C1, C2–N1–C4 and C1–N1–C4 are also near 120° (119.56°, 121.08° and 116.72°, respectively).[26]

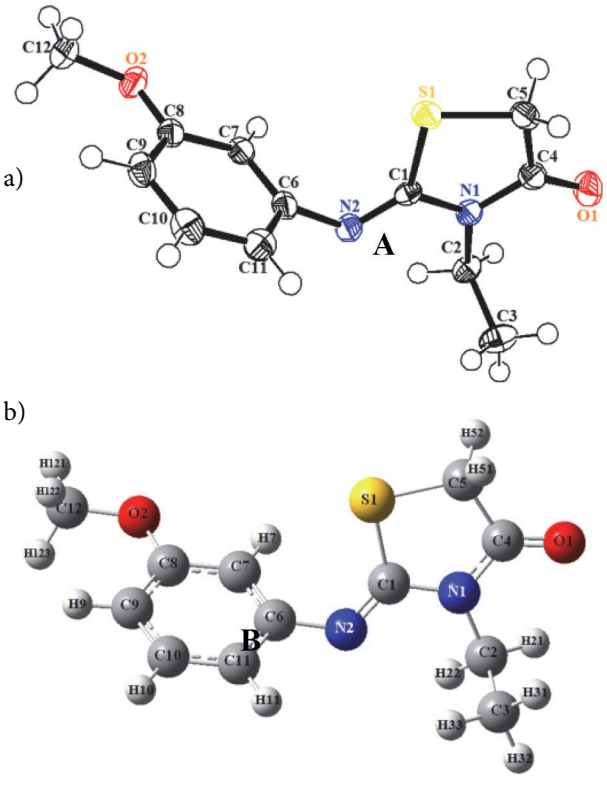

Figure 1. Experimental (a) and theoretical (b) structure of (*Z*)-3-*N*-(ethyl)-2-*N*'-((3-methoxyphenyl)imino)thiazolidine-4-one.

The bond angles centered on C1 are all between 109° and 129°. The C1 atom is of sp^2 hybridization type because the total adds up to 360° at B3LYP/6-311G(d,p) level. The corresponding theoretical values of this angle is 64° (C7–C6–N2–C1). The C8–O2–C12 angle is 116.98°, and the C2–N1–C4–O1 fragment is approximately planar (Table 4).

Generally, the observed difference between experimental and calculated geometrical parameters does not seem very large.

Table 2. Experimental and optimized bond lengths (Å).

Bond lengths	X-ray	B3LYP/6-311G(d,p)
S1–C5	1.811(1)	1.887
S1–C1	1.767(1)	1.893
O1–C4	1.216(1)	1.233
N1–C2	1.469(1)	1.485
N1–C1	1.399(1)	1.392
N1–C4	1.371(1)	1.388
N2–C6	1.425(1)	1.407
N2–C1	1.263(1)	1.264
O2–C8	1.367(1)	1.386
O2–C12	1.431(1)	1.459
C6–C7	1.389(1)	1.398
C6–C11	1.402(1)	1.408
C7–C8	1.398(1)	1.401
C5–C4	1.509(1)	1.527
C2–C3	1.518(1)	1.537
C10–C9	1.393(1)	1.399
C10–C11	1.386(1)	1.387
C8–C9	1.395(1)	1.397

Table 3. Experimental and optimized bond angles (°).

Bond angles	X-ray	B3LYP/6-311G(d,p)
C5–S1–C1	92.24	90.13
C2–N1–C1	122.15	120.13
C2–N1–C4	121.08	119.58
C1–N1–C4	116.72	29.83
C6–N2–C1	119.56	129.18
C8–O2–C12	116.98	117.97
N2–C6–C7	119.43	124.07
N2–C6–C11	119.94	116.82
C7–C6–C11	120.34	119.08
C6–C7–C8	119.87	120.72
S1–C5–C4	107.51	108.27
N1–C2–C3	112.36	111.42
S1–C1–N1	110.92	109.07
S1–C1–N2	127.32	129.12
N1–C1–N2	121.76	121.81
O1–C4–N1	123.71	123.73
O1–C4–C5	123.91	124.08
N1–C4–C5	112.37	112.18
C9–C10–C11	121.52	120.98
O2–C8–C7	115.23	115.22
O2–C8–C9	124.48	124.87
C7–C8–C9	120.27	119.91
C10–C9–C8	119.01	119.34
C6–C11–C10	118.98	119.96

Table 4. Experimental and optimized torsion angles (°).

Torsion angles	X-ray	B3LYP/6-311G(d,p)
C1–S1–C5–C4	3.6	2.4
C5–S1–C1–N1	–4.7	–2.4
C5–S1–C1–N2	174.5	176.7
C1–N1–C2–C3	–99.6	–86.2
C4–N1–C2–C3	77.9	92.2
C2–N1–C1–S1	–177.7	–179.7
C2–N1–C1–N2	3.1	1.1
C4–N1–C1–S1	4.7	1.8
C4–N1–C1–N2	–174.6	–177.3
C2–N1–C4–O1	–0.2	1.7
C2–N1–C4–C5	–179.5	–178.4
C1–N1–C4–O1	177.4	–179.9
C1–N1–C4–C5	–1.9	0.1
C1–N2–C6–C7	86.0	64.5
C1–N2–C6–C11	–100.2	–119.3
C6–N2–C1–S1	1.6	4.4
C6–N2–C1–N1	–179.2	–176.7
C12–O2–C8–C7	–170.8	179.8
C12–O2–C8–C9	10.9	–0.1
N2–C6–C7–C8	172.3	178.5
C11–C6–C7–C8	–1.5	0.6
N2–C6–C11–C10	–173.1	–179.4
C7–C6–C11–C10	0.6	–1.3
C6–C7–C8–O2	–177.2	–179.5
C6–C7–C8–C9	1.3	0.4
S1–C5–C4–O1	178.9	178.06
S1–C5–C4–N1	–1.8	–1.9
C11–C10–C9–C8	–0.8	–0.1
C9–C10–C11–C6	0.5	1.1
O2–C8–C9–C10	178.2	179.2
C7–C8–C9–C10	–0.1	–0.7

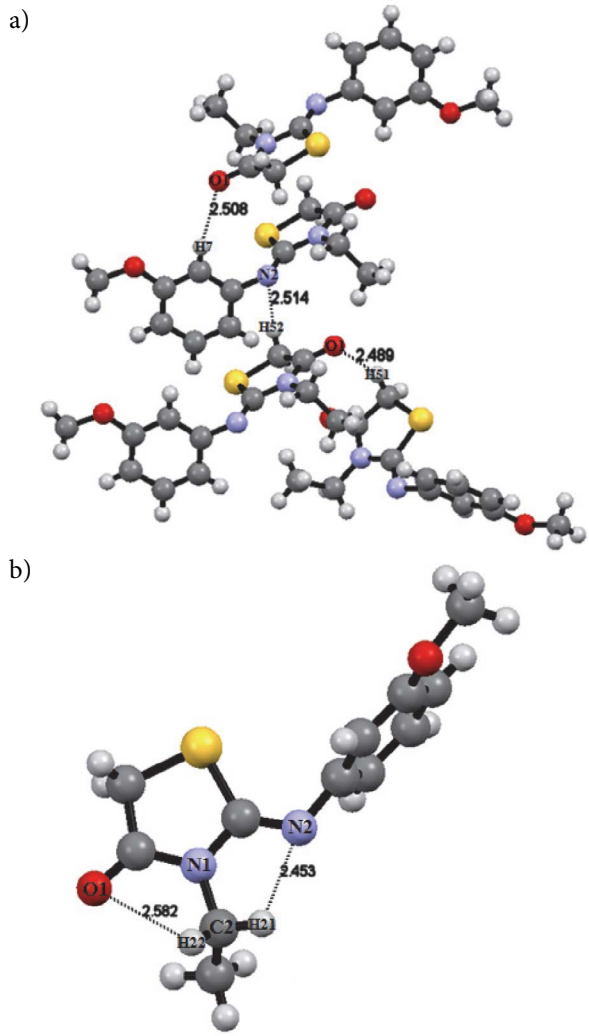

Figure 2. Hydrogen bonding view in the crystal showing: (A) intermolecular interactions, (B) C2–H21···N2 and C2–H22···O1 intramolecular interactions.

4. 2. Hydrogen Bonding

Hydrogen bonds join chains of molecules to stabilize the crystal structure of the title compound. Along the *b* axis in the unit cell, the translation of equivalent molecules allows the linking of the almost linear hydrogen bonding. C–H···O and C–H···N intra- and intermolecular interactions are present in the crystal structure. The molecular conformation is in part influenced by the formation of two weak intramolecular C2–H22···O1 and C2–H21···N1 hydrogen bonds that enclose S(5) rings (Figure 2 and Table 5).

These interactions are responsible for the stability of the molecular packing, as the C2, C3, C5, C12 and C7 carbon atoms act as donor groups and both oxygen and nitrogen atoms play the acceptor role. Hydrogen bond interactions are presented in Table 5. Figure 2 shows all interaction types in the crystal. The molecular stacking that has been provided by the different existing hydrogen bonds in the

Table 5. Geometry of the C–H···O and C–H···N hydrogen bonds in (*Z*)-3-*N*-(ethyl)-2-*N*'-((3-methoxyphenyl)imino)thiazolidine-4-one crystal by X-ray diffraction.

D–H···A	D–H (Å)	D–A (Å)	H···A (Å)	D–H···A (°)	Bond type
C2–H21···N2	0.981	2.852	2.453	103.88	Intramolecular
C2–H22···O1	0.962	2.817	2.582	93.97	Intramolecular
C5–H51···O1$^{(i)}$	0.987	3.380	2.489	149.92	Intermolecular
C7–H7···O1$^{(ii)}$	0.947	3.432	2.508	164.98	Intermolecular
C5–H52···N2$^{(iii)}$	0.955	3.370	2.514	149.26	Intermolecular

Symmetry codes: *(i)* –*x*, *y*, –*z* + 1/2; *(ii)* –*x*, –*y*, –*z*; *(iii)* *x*, –*y*, *z* + 1/2

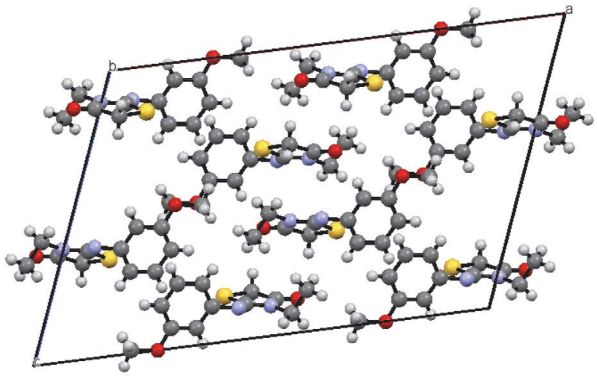

Figure 3. View of the crystal packing along the *b* axis of (*Z*)-3-*N*-(ethyl)-2-*N*'-((3-methoxyphenyl)imino)thiazolidine-4-one molecule.

crystal is shown in Figure 3. This figure shows the existence of eight molecules in the unit cell which is in good agreement with the multiplicity of the space group C2/c.

4. 3. Vibrational Frequencies Assignments

Using analytic second derivatives to validate the convergence to minima on the potential energy surface the fundamental frequencies of the studied molecule have been calculated to understand the nature of these modes of vibration IR absorption spectroscopy based on DFT calculation. A theoretical analysis has been realized using B3LYP/6-311G(d,p) level of theory in gas phase. The probable assignments were performed by means of VEDA 4 program.[23] The vibrational frequencies obtained from B3LYP functional calculations have been scaled by a factor of 0.967.[27] Table 6 shows the calculated (unscaled and scaled) and experimental frequencies of the title compound. Simulated and experimental IR spectra of (*Z*)-3-*N*-(ethyl)-2-*N*'-((3-methoxyphenyl)imino)thiazolidine-4-one are shown in Figure 4. As can be seen in Figure 4, the experimental fundamentals are in better agreement with the scaled fundamentals.

4. 3. 1. Carbon–Hydrogen Vibrations

In the aromatic compounds, multiple weak bands are exhibited in the region of 3100–3000 cm^{-1}.[28] They appear in this range of like multiple weak bands due to the stretching vibrations of C–H.[29] In the present work, the carbon–hydrogen of aromatic ring (C–H) stretching (νCH modes) were found in a range of 3000 and 3100 cm^{-1} using the B3LYP/6-311G(d,p) calculations. These modes involve exact contribution of >91% suggesting that they are pure stretching modes. The C–H stretching of aromatic ring showed symmetric modes at 3001, 3070 and 3080 cm^{-1} while asymmetric stretching mode was observed at 2989 cm^{-1}.

4. 3. 2. C=O and C=N Vibrations

Usually, the C=O stretching vibration mode can be easily observed as a strong band in the region 1850–1550 cm^{-1}.[30] The π–π bonding between carbon and oxygen is responsible for forming a double bond between the carbon and oxygen atoms. The electronic distribution in this link is not equal because these atoms have different electronegativities. The lone pair of electrons on oxygen is responsible for the polar nature of the carbonyl group. In the present study, the single C=O stretching vibration mode was observed as a high-intense peak in FT-IR at 1716 cm^{-1} while the calculated value shows at 1726 cm^{-1} with a PED (potential energy distribution) of 79%. The stretching frequency of the double bond C=N is perfectly observed at the high absorption 1640 cm^{-1}. DFT/B3LYP functional with 6-311G(d,p) basis set gives exactly the same value of 1640 cm^{-1} for the C=N vibration.

4. 3. 3. Thiazolidine Ring Vibrations

The C–S stretching vibration presents average bands in the region 1020–1010 cm^{-1}.[31] In this paper C–S vibrations were observed at 704, 647 and 526 cm^{-1}. The examination of the theoretical results gives us the following values with their PED contribution: 720 (21%), 642 (10%), 522 (12%) and 482 (23%) respectively, which shows a good agreement between theoretical and experimental ones as shown in the Table 6. C–N vibration is a difficult task to identify since the appearance of several bands is possible in the region, Gunasekaran *et al.*[32] have observed C–N stretching band at 1312 cm^{-1},[33] and C–N assigned stretching vibration in the region 1350–1000 cm^{-1} for amines. In thiazolidine, C–N stretching band is found to be present at 1382 and 1307 cm^{-1}. The C–N stretching vibrations are expected to occur in the region 1200–1130 cm^{-1}.[34] In our present work of the title molecule FTIR bands were observed at 896 cm^{-1} and 1234 cm^{-1}, the theoretically calculated bands at 940, 1405, 1357, 1301, 1257, 1131 are shifted

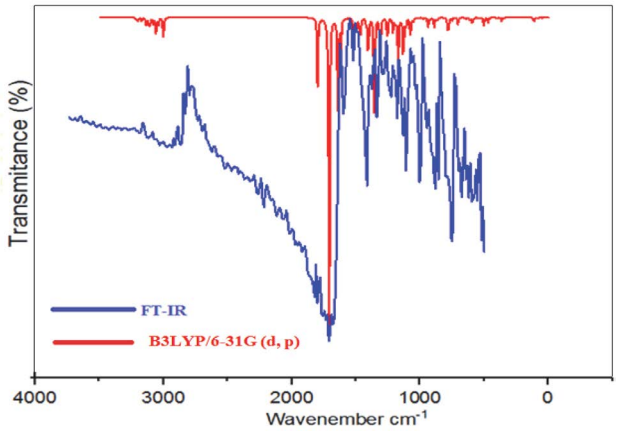

Figure 4. Comparison of FT-IR and calculated IR Spectra for (*Z*)-3-*N*-(ethyl)-2-*N*'-((3-methoxyphenyl)imino)thiazolidine-4-one.

Table 6. Comparison of the calculated harmonic frequencies using B3LYP method 6-311G(d,p) basis set and experimental (FT-IR) wavenumbers (cm^{-1}) for (*Z*)-3-*N*-(ethyl)-2-*N'*-((3-methoxyphenyl)imino)thiazolidine-4-one.

No	Experimental	B3LYP/6-311G(d,p) Unscaled	Scaled	I_{IR}	Assignments with PED>10%
87		3209	3080.64	8.75	ν CH (91%) Ar ring
86		3198	3070.08	0.77	ν CH (92%) Ar ring
85		3127	3001.92	9.61	ν CH (100%) Ar ring
83		3139	3013.44	9.25	ν CH (79%) + ν_{as} CH (11%)
81		3127	3001.92	0.33	ν CH (100%)
80	2971	3114	2989.44	13.61	ν_{as} CH (92%)
74		3001	2880.96	61.94	ν CH (92%)
73	1716	1798	1726.08	182.70	ν C=O (79%)
72	1640	1709	1640.64	943.72	ν N=C (73%)
71		1640	1574.4	329.64	ν CC_{asy} (63%) Ar ring +δ HCC (14%) Ar ring
70		1617	1552.32	93.33	ν CC (51%)$_{asy}$ Ar ring+ δ HCC (11%) Ar ring+ δ CCC (12%) Ar ring
69	1482	1518	1457.28	72.82	δ HCC_{asy} (44%) Ar ring+ δ CCC (19%) Ar ring
68		1508	1447.68	33.99	δ HCH (67%)+
67		1506	1445.76	3.59	δ HCH(71%)+ τ$HCCN_{asy}$ (22%) Th ring
66		1498	1438.08	8.56	δ HCH(71%)+ τ$HCCN_{asy}$ (24%) Th ring
65		1492	1432.32	7.71	δ HCH_{asy}(69%)+ τ$HCOC_{asy}$(24%) Ar ring
64		1482	1422.72	0.82	δ HCH(48%)
62		1465	1406.4	40.95	ν CC_{asy} (31%) Ar ring+ δ HCC (31%) Ar ring+ δ HCC_{asy} (16%)
61		1462	1403.52	8.14	δ HCH (88%)
60	1391	1420	1363.2	18.06	δ HCC (13%)+ δ HCH (15%)+ τHCNC (46%) Th ring
59		1405	1348.8	110.90	ν NC(13%) Th ring+ δ HCC (10%)+ δ HCH (39%)+ τ$HCNC_{asy}$ (10%) Th ring
58		1401	1344.96	12.94	δ HCC (56%)+ δ HCH (14%)
57		1357	1302.72	247.21	ν NC(46%) Th ring
56	1284	1350	1296	24.41	ν CC_{asy} (59%) Ar ring+ δ HCC (23%)
55		1312	1259.52	111.70	ν CO_{asy}(79%) Ar ring+ δ HCC (37%) Ar ring
54	1234	1301	1248.96	13.79	ν CC (10%) Ar ring+ ν NC_{th}(12%) Ar ring+ δ HCC (11%) Ar ring+ δ HCH_{asy} (14%)
53		1257	1206.72	43.11	ν NC_{asy} (16%)+ Th ring +ν CO(13%) Ar ring+ τHCCN (12%) Th $ring_{asy}$
52		1253	1202.88	25.58	τ$HCSC_{asy}$(84%) Th ring
51		1212	1163.52	40.44	δ HCH_{asy}(15%)+ τHCOC(44%) Ar ring
50	1148	1194	1146.24	22.35	ν CC (10%) Ar ring+ δ HCC (38%) Ar ring+ τ$HCOC_{asy}$(14%) Ar ring
49		1172	1125.12	45.03	δ HCH(21%)+ τHCOC(35%) Ar ring
48		1171	1124.16	101.55	δ HCC_{asy} (13%) Ar ring+ τ$HCOC_{asy}$(17%) Ar ring
47		1148	1102.08	3.08	δ HCS_{asy} (52%) Th ring+ τHCSC(28%) Th ring
46		1131	1085.76	146.72	ν NC_{asy} (15%) Th ring+ ν CC(11%) Th ring
45		1111	1066.56	17.22	δ HCH_{asy}(12%)+ δ CCN_{asy} (13%) Th ring+ τHCCN (36%) Th $ring_{asy}$
44		1109	1064.64	12.00	ν CC(14%) Ar ring+ δ HCC(33%) ar ring+
43	1046	1075	1032	63.45	ν OC(55%) Ar ring+ δ HCC(17%) Ar ring
41		1007	966.72	0.82	ν CC_{asy} (52%) Ar ring+ δ CCC_{asy}(39%) Ar ring
40		973	934.08	4.63	ν CC_{asy} (33%) Th ring
39	927	968	929.28	0.03	τHCCC (77%) Ar ring
38	896	940	902.4	27.82	ν NC(10%) Ar ring+ ν OC_{asy}(10%) Ar ring+ ν CC_{asy} (27%) Th ring
37		922	885.12	7.21	δ HCS(45%) Th ring+ τHCSC (21%) Th ring+ τ$CCNC_{asy}$(19%) Th ring+ γ $OCNC_{asy}$(15%)
36		891	855.36	29.40	ν CC_{asy} (12%) Th ring+ δ NCN_{asy} (10%)+ τHCCC (12%) Ar ring
35		872	837.12	7.58	τHCCC (68%) Ar ring
34		863	828.48	5.52	τHCCC (68%) Ar ring
33	775	791	759.36	5.21	δ NCN_{asy} (32%) Th ring+ τHCNC (33%) Th ring
32		782	750.72	30.71	τHCCC (17%) Ar ring+ τ$HCCC_{asy}$ (17%) Ar ring+τ$CCCC_{asy}$(29%) Ar ring
31	740	779	747.84	20.41	δ CNC (27%) Th ring
30	704	751	720.96	8.75	ν CC_{asy} (10%) Ar ring+ ν CC(10%) Th ring+ ν SC(21%) Th ring
29		705	676.8	22.45	τ$HCCC_{asy}$ (56%) Ar ring+ τ$CCCC_{asy}$(10%) Ar ring
28	647	669	642.24	0.28	ν SC(10%) Th ring+ τ$HCCC_{asy}$ (12%) Ar ring+ τCCCC(43%) ar ring
27	609	643	617.28	4.95	ν CC(28%) Th ring+ δ CCC_{asy}(11%) Ar ring

26		617	592.32	4.44	γSNNC $_{asy}$(54%) Ar ring
25	584	610	585.6	5.88	δ CNC$_{asy}$ (11%) Th ring
24		593	569.28	17.41	δ CCC$_{asy}$ (14%) Ar ring+ γOCNC(19%) Th ring
23		581	557.76	1.53	τHCSC$_{asy}$ (16%) Th ring+ γOCNC$_{asy}$ (30%) Th ring
22	526	544	522.24	3.20	ν SC(12%) Th ring+ δ CCC (25%) Ar ring+ τCCCC (12%) Ar ring
21		503	482.88	23.21	ν SC$_{asy}$ (23%) Th ring+ δ CCN$_{asy}$(14%) Ar ring
20		484	464.64	0.63	δ CNC$_{asy}$(10%) Ar ring+ δ CCO$_{asy}$(32%) Ar ring
19		471	452.16	16.37	δ CNC$_{asy}$(19%) Th ring+ δ CCN$_{asy}$(16%) Th ring+ δ CCO$_{asy}$(12%) Th ring
18		454	435.84	1.08	δ CCO$_{asy}$(11%) Ar ring+ τCCCC$_{asy}$ (36%) Ar ring
17		403	386.88	2.62	δ CCC(12%) Ar ring+ δ COC$_{asy}$ (21%) Ar ring

ν: stretching(elongation); sy: symmetric; asy: asymmetric; β: in plane bending; γ: out-of-plane bending, ω: wagging; τ: twisting; δ: bending; ρ: rocking; vibrational modes are based on potential energy distribution (PED) and only contributions over 10% are given; scaled frequencies are in unit of cm^{-1}; I_{IR} infrared intensities are in unit of km mol^{-1}.

down by scaling the previous values to 902 (10%), 1348 (13%), 1302 (46%), 1248 (12%), 1206 (16%), 1085 (15%), respectively with the percentage of the PED contribution indicated between brackets.

4. 4. ^{1}H and ^{13}C NMR Calculations

To calculate isotropic chemical shifts (δ) with respect to tetramethylsilane (TMS): $\delta^x_{iso} = \sigma^{TMS}_{iso} - \sigma^{x}_{iso}$,[34] isotropic shielding values 184.2796 and 32.2899 ppm of σ^{TMS}_{iso} were used for C and H NMR spectra, respectively. It is known that the range of ^{13}C NMR chemical shifts for analogous organic molecules usually are >100 ppm.[35,36] Methanol solvent has been used for chemical shift measurements. The atoms were labeled according to the numbering presented in Figure 1 (B). Calculated and experimental values for ^{1}H and ^{13}C NMR are collected in Table 7. In this research, aromatic carbons give signals in overlapped areas of the spectrum with chemical shift values from 106 to 170 ppm while experimental chemical shift values of aromatic carbon atoms are in the range 107 to 160 ppm as they would be expected (Table 7). Carbon atoms (C1, C4 and C6) attached to the N atom have larger chemical shifts due to the more electronegative property of the N atom which polarizes the electron distribution in its binding to the atom adjacent carbon and reduces the value of the chemical shifts. Usually, the chemical shifts obtained and calculated for the ^{1}H atoms of the methyl groups are quite weak. The maximum chemical shift value for all the hydrogen atoms is 7.24 ppm.

Table 7. Experimental and calculated ^{1}H and ^{13}C NMR data for (*Z*)-3-*N*-(ethyl)-2-*N*'-((3-methoxyphenyl)imino)thiazolidine-4-one.

Chemical shifts		
^{1}H	Experimental	B3LYP/6-311G(d)
H_{51}	3.78	4.03
H_{52}	3.78	3.94
H_{21}	3.90	4.49
H_{22}	3.90	4.25
H_{31}	1.29	1.02
H_{32}	1.29	1.92
H_{33}	1.29	1.19
H_9	6.52	6.26
H_7	6.67	6.71
H_{11}	6.56	6.64
H_{10}	7.24	7.42
H_{121}	3.79	4.32
H_{122}	3.79	3.74
H_{123}	3.79	3.73
^{13}C		
C1	154.23	158.27
C2	32.76	37.78
C3	12.52	15.06
C4	171.55	176.61
C5	38.26	37.57
C6	149.32	158.15
C7	110.39	113.89
C8	160.37	170.89
C9	107.22	106.29
C10	129.99	136.22
C11	113.20	120.10
C12	55.25	58.70

4. 5. Frontier Molecular Orbitals (FMOs)

The highest occupied molecular orbitals (HOMO) and the lowest unoccupied molecular orbitals (LUMO) are named as frontier molecular orbitals (FMO). The HOMO represents the ability to donate an electron, whereas LUMO as an electron acceptor represents the ability to obtain an electron.[37] The calculation of these parameters is very important because it allowed us to verify a lot of properties, such as the kinetic stability and chemical reactivity. Figure 5 shows the atomic orbital HOMO–LUMO plot of the frontier molecular orbitals computed at B3LYP/6-311G(d,p) level for the title compound. As shown in Figure 5, in HOMO density, electrons are mainly located on the methoxyphenyl group. However, when an electron transition occurs, the electron enters into the LUMO, and then the electron will mainly be localized on thiazole ring and carboxylic group. The positive phase is red and the negative one is green coloured. The HOMO–

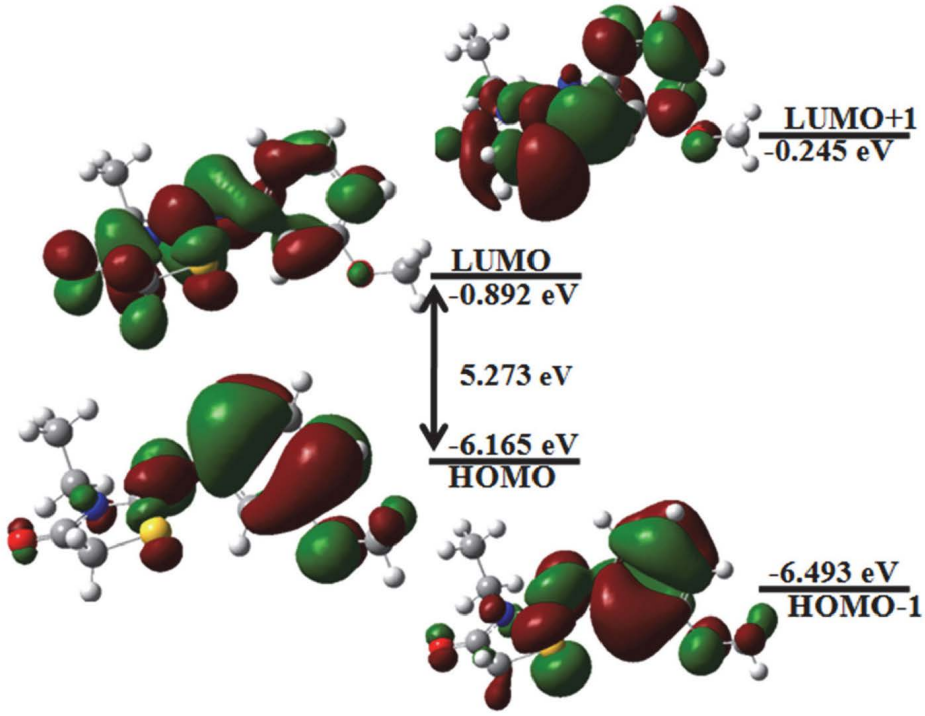

Figure 5. Electron distribution of the HOMO–1, HOMO, LUMO and LUMO+1 energy levels for the title molecule.

LUMO energy gap of our molecule was calculated at the B3LYP/6-311G (d,p) level with HOMO energy –6.165 eV, LUMO energy –0.892 eV and HOMO–LUMO energy gap 5.273 eV. The second highest occupied MO (HOMO–1) and the second lowest unoccupied MO (LUMO+1) were calculated using the same level of theory. 3D plots of the HOMO–1, HOMO, LUMO and LUMO+1 orbitals of the studied molecule are drawn in Figure 4.

4. 6. Chemical Reactivity

Global chemical reactivity descriptors (GCRD) parameters are a good indication to highlight the relationship between chemical reactivity and strength of structure. As are mentioned in literature, GCRD parameters can be obtained by using the following equations: $\eta = \frac{1}{2}(E_{LUMO}-E_{HOMO})$; $\mu = -\left(\frac{I+A}{2}\right)$; $S = \frac{1}{2\eta}$; $\chi = \left(\frac{I+A}{2}\right)$; $\omega = \frac{\mu^2}{2\eta}$. $A = -E_{LUMO}$ and $I = -E_{HOMO}$. The electron affinity (A) and ionization potential (I) can be evaluated as and . The calculated values of GCRD parameters for the title molecule are summarized in Table 8.

The chemical hardness (η) value is 2.636 eV indicating that the charge transfer occurs within the molecule. From Table 8, the electrophilic behaviour of the molecule is confirmed by the global electrophilicity index (ω) which has a greater value of 2.361 eV. On the other hand, the chemical stability of the title molecule is explained by the chemical potential (μ) value which is –3.528 eV.

Table 8. Calculated energy values of the title compound by B3LYP/6-311G(d,p) method.

Parameters	Calculated energies
E_{HOMO}	–6.165
E_{LUMO}	–0.892
Energy gap (ΔE)	5.273
Ionization potential (I)	6.165
Electron affinity (A)	0.892
Electronegativity (χ)	3.528
Chemical potential (μ)	–3.528
Chemical hardness (η)	2.636
Chemical softness (s)	0.189
Electrophilicity index (ω)	2.361

4. 7. Electrostatic Potential

In a crystal, the location of positive and negative charges allowed us to define very interesting physical properties such as the molecular electrostatic potential (MEP).[38] Nowadays, theoretical and experimental MEP surfaces are determined using quantum chemistry and X-ray diffraction.[39–42] The MEP around the title molecule was calculated from the total density (TD) for the title compound, the two maps (TD and MEP) are represented in the Figure 6. From the figure it can be seen that the negative MEP is related to the electronegativity and partial charges of oxygen atoms O1 and O2. The blue color in Figure 6B gives the maximum positive region as the preferred

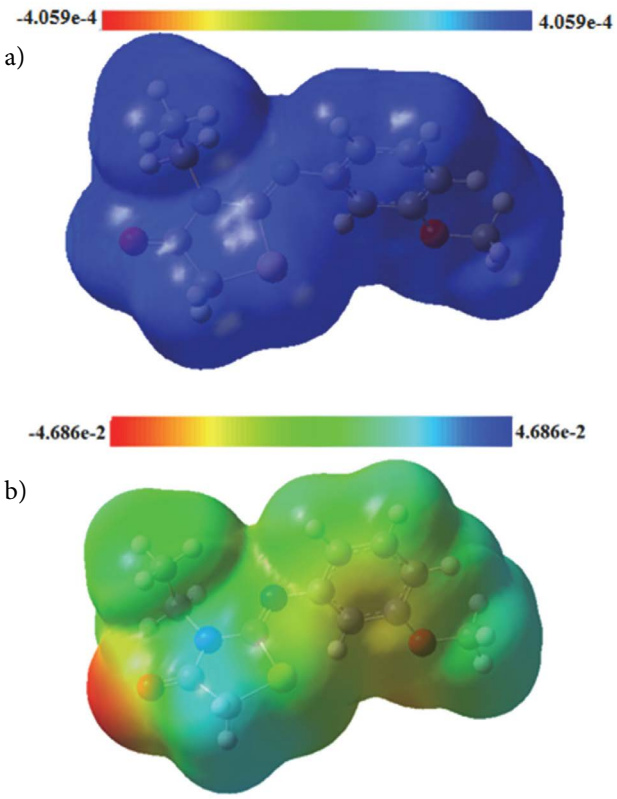

Figure 6. MEP plots for (*Z*)-3-*N*-(ethyl)-2-*N*'-((3-methoxyphenyl) imino)thiazolidine-4-one: (a) total electron density, (b) MEP surface.

site for nucleophilic attack. In terms of color, the MEP plot lies in the fact that it simultaneously displays molecular size, shape as well as positive, negative and neutral electrostatic potential regions (Figure 6). The MEP indicate well the relationship between the molecular structure and these physico-chemical properties.[43–47] Among them, the molecular dipole moment can be calculated. The orientation of the molecular dipole moment for the title compound is represented in Figure 7. This orientation confirms the electrostatic distribution previously defined. The calculated dipole moment value is 2.24 D.

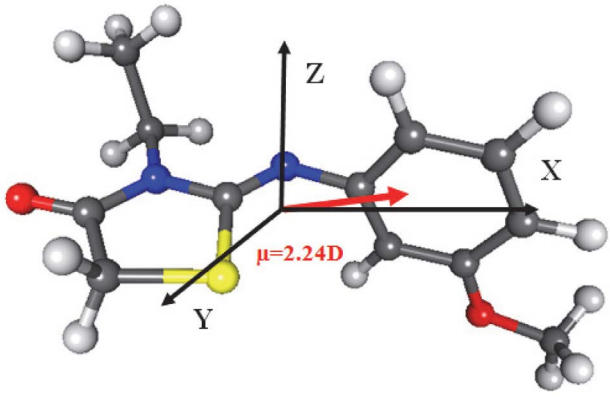

Figure 7. Orientation of the molecular dipole moment from DFT calculation.

5. Conclusion

In this study, (*Z*)-3-*N*-(ethyl)-2-*N*'-((3-methoxyphenyl)imino)thiazolidine-4-one was synthesized and characterized by IR, ^{1}H and ^{13}C NMR and X-ray single-crystal diffraction techniques. The crystal structure determination shows that the title compound crystallizes in monoclinic system with space group C2/c. Theoretical calculations of the molecular structures, wavenumbers and NMR spectra of the title compound have been carried out using DFT-B3LYP/6-311G(d,p). As result, the experimental and the optimized crystal structures of the title compound were slightly different. Most of the experimental bond lengths and bond angles are slightly larger than the optimized values. These differences are due to that the theoretical calculations are performed for isolated molecule in gaseous phase and the experimental results are for a molecule in the crystalline environment. The geometry of the solid-state structure is subject to intermolecular forces, such as Van der Waals interactions and crystal packing contacts. Comparison between the chemical shifts and the experimental data shows a very good agreement for both ^{1}H and ^{13}C NMR shift values. The HOMO–LUMO gap and chemical reactivity descriptors indicate that the compound is more stable. The general conclusion from the estimation of the dipolar moment (2.24 D) and the electrostatic potential of ((*Z*)-3-*N*-(ethyl)-2-*N*'-((3-methoxyphenyl)imino)thiazolidine-4-one molecule is that the region of the thiazolidinone group is electronegative and the methyl and hydrogen atoms connected to the benzene ring are electropositive.

6. Supplementary Material

Crystallographic data for the structure reported in this article have been deposited with Cambridge Crystallographic Data Center, CCDC 1871013. Copies of this information may be obtained free of charge from the Director, CCDC, 12 Union Road, Cambridge, CB2 1EZ, UK. Facsimile (44) 01223 336 033, E-mail: deposit@ccdc.cam.ac.uk or http//www.ccdc.com.ac.uk/deposit.

7. References

1. J. Quiroga, P. Hernandez, B. Insuasty, R. Abonia, J. Cobo, A. Sanchez, M. Nogueras, *J. Chem. Soc. Perkin Trans. 1* **2002**, *4*, 555–559. **DOI:**10.1039/b109676a
2. I. Hutchinson, S. A. Jennings, B. R. Vishnuvajjala, A. D. Westwell, M. F. G. Stevens, *J. Med. Chem.* **2002**, *45*, 744–747. **DOI:**10.1021/jm011025r

3. R. I. Bahoussi, A. Djafri, A. Chouaih, A. Djafri, F. Hamzaoui, *Acta Cryst*. **2017**, *E73*, 173–176. **DOI:**10.1107/S205698901700041X
4. A. Srinivas, M. Sunitha, P. Karthik, K. V. Reddy, *Acta Chim. Slov.* **2017**, *64*, 1030–1041. **DOI:**10.17344/acsi.2017.3805
5. K. D. Hargrave, F. K. Hess, J. T. Oliver, *J. Med. Chem*. **1983**, *26, 1158*–1163. **DOI:**10.1021/jm00362a014
6. W. C. Patt, H. W. Hamilton, M. D. Taylor, M. J. Ryan, J. R. Taylor, C. J. C. Connolly, *J. Med. Chem.* **1992**, *35*, 2562–2572. **DOI:**10.1021/jm00092a006
7. R. N. Sharma, F. P. Xavier, K. K. Vasu, S. C. Chaturvedi, S. S. Pancholi, *J. Enz. Inhib. Med. Chem.* **2009**, *24*, 890–897. **DOI:**10.1080/14756360802519558
8. J. C. Jaen, L. D. Wise, B. W. Caprathe, H. Tecle, S. Bergmeier, C. C. Humblet, T. G. Heffner, *J. Med. Chem.* **1990**, *33*, 311–317. **DOI:**10.1021/ jm00163a051
9. K. Tsuji, H. Ishikawa, *J. Med. Chem. Lett*. **1994**, *4*, 1601–1606. **DOI:**10.1016/S0960-894X(01)80574-6
10. F. W. Bell, A. S. Cantrell, M. Hogberg, S. R. Jaskunas, N. G. Johansson, C. L. Jordon, *J. Med. Chem*. **1995**, *38*, 4929–4936. **DOI:**10.1021/jm00025a010
11. N. Ergenc, G. Capan, N. S. Gunay, S. Ozkirimli, M. Gungor, S. Ozbey, E. Kendi, *Arch. Pharm*. **1999**, *332*, 343–347. **DOI:**10.1002/ (SICI)1521-4184(199910)332:10<343::AID -ARDP343>3.0.CO;2-0
12. J. S. Carter, S. Kramer, J. J. Talley, T. Penning, P. Collins, M. J. Graneto, K. Eibert, *Bioorg. Med. Chem. Lett*. **1999**, *9*, 1171–1174. **DOI:**10.1007/s00706-010-0392-3
13. A. Badorc, M. F. Bordes, P. De Cointet, P. Savi, A. Bernat, A. Lale, M. Petitou, *J. Med. Chem.* **1997**, *40*, 3393–3401. **DOI:**10.1021/jm970240y
14. G. Aridoss, S. Amirthaganesan, M. S. Kim, J. T. Kim, Y. T. Jeong, *Eur. J. Med. Chem*. **2009**, *44*, 4199–4210. **DOI:**10.1016/j.ejmech.2009.05.015
15. Bruker Analytical X-ray Systems, Inc, Apex2, Version 2 User Manual, M86–E01078, **2006**, 6, Madison, WI.
16. Siemens Industrial Automation, Inc. SADABS: Area-Detector Absorption Correction, **1996**, Madison, WI.
17. P. W. Betteridge, J. R. Carruthers, R. I. Cooper, K. Prout, D. J. Watkin, *J. Appl. Crystallogr*. **2003**, *36*,1487. **DOI**:10.1107/S0021889803021800
18. L. Palatinus, G. Chapuis, *J. Appl. Crystallogr*. **2007**, *40*, 782–785. **DOI**:10.1107/S002188980702420X
19. C. Jelsch, B. Guillot, A. Lagoutte, C. Lecomte, *J. Appl. Crystallogr*. **2005**, *38*, 38–54. **DOI:**10.1107/S0021889804025518
20. A. D. Becke, *J. Chem. Phys*. **1997**, *107*, 8554–8560. **DOI:**10.1063/1.475007
21. P. C. R. Kumar, V. Ravindrachary, K. Janardhana, B. Poojary, *J. Cryst. Growth* **2012**, *354*, 182–187. **DOI:**10.1016/j.jcrysgro.2012.06.006
22. A. Frish, A. B. Nielsen, A. J. Holder, Gaussview Users Manual, Gaussian Inc, Pittsburg, **2000**.
23. M. H. Jamróz, J. C. Z. Dobrowolski, *J. Mol. Struct*. **2001**, *565*, 475–480. **DOI:**10.1016/S0022-2860(00)00908-X
24. L. J. Farrugia, "ORTEP-3 for windows-a version of ORTEPI-II with a graphical user interface (GUI), *J. Appl. Crystallogr*. **1997**, *30*, 565–568. **DOI:**10.1107/S0021889897003117
25. S. Yahiaoui, A. Moliterni, N. Corriero, C. Cuocci, K. Toubal, A. Chouaih, A. Djafri, F. Hamzaoui, *J. Mol. Struct*. **2019**, *1177*, 186–192. **DOI:**10.1016/j.molstruc.2018.09.052
26. N. Khelloul, K. Toubal, N. Benhalima, R. Rahmani, A. Chouaih, A. Djafri, F. Hamzaoui, *Acta. Chim. Slov*. **2016**, *63*, 619–626. **DOI:**10.17344/acsi.2016.2362
27. S. P. V. Chamundeeswari, E. R. J. J. Samuel, N. Sundaraganesan, *Eur. J. Chem*. **2011**, *2*, 136–145. **DOI:**10.5155/eurjchem.2.2.136-145.169
28. A. Eşme, S. Güneşdoğdu Sağdınç, *Spectrochim. Acta A Mol. Biomol. Spectrosc*. **2018**, *188*, 443–455. **DOI:**10.1016/j.saa.2017.07.034
29. G. Muhammad, A. Muhammad, A. M. Khalid, *J. Mol. Struct*. **2018**, *1160*, 129–141. **DOI:**10.1016/j.molstruc.2018.01.100
30. P. K. Murthy, G. Krishnaswamy, S. Armaković, S. J. Armaković, P. A.Suchetan, N. R. Desai, V. Suneetha, R. Sreenivasa Rao, G. Bhargavi, D. B. Arunakumar, *J. Mol. Struct*. **2018**, *1162*, 81–95. **DOI:**10.1016/j.molstruc.2018.02.081
31. A. Teimouri, A. N. Chermahini, M. D. Emami, *Arkivoc* **2008**, *8*, 172–187.
32. H. Dammak, A. Yangui, S. Triki, Y. A. H. Feki, *J. Lumin.* **2015**, *161*, 214–220. **DOI:**10.1016/j.jlumin.2015.01.010
33. M. Silverstein, G. C. Basseleer, C. Moril, Spectrometric Identification of Organic Compounds, Wiley, New York, **1981**.
34. S. Muthu, J. U. Maheswari, T. Sundius, *Spectrochim. Acta A Mol. Biomol. Spectrosc*. **2013**, *108*, 307–318. **DOI:**10.1016/j.saa.2013.02.022
35. G. Socrates, Infrared Characteristic Group Frequencies, Wiley Inter Science Publication, 1980.
36. G. Varsanyi, Vibrational Spectra of Benzene Derivates, Academic Press, New York, 1969.
37. K. Toubal, N. Boukabcha, Ö. Tamer, N. Benhalima, S. Altürk, D. Avcı, A. Chouaih, Y. Atalay, A. Djafri, F. Hamzaoui, *J. Mol. Struct*. **2017**, *1147*, 569–581. **DOI:**10.1016/j.molstruc.2017.06.102
38. R. Rahmani, N. Boukabcha, A. Chouaih, F. Hamzaoui, S. Goumri, *J. Mol. Struct*. **2018**,*1155*, 484–495. **DOI:**10.1016/j.molstruc.2017.11.033
39. H. Benaissi, M. Drissi, S. Yahiaoui, Y. Megrouss, A. Chouaih, F. Hamzaoui, *J. Optoelectron. Biomed. M*. **2018**, *10*, 73–82
40. N. Boukabcha, A. Feddag, R. Rahmani, A. Chouaih, F. Hamzaoui, *J. Optoelectron. Adv. M.* **2018**, *20*, 140–148
41. N. Boubegra, Y. Megrouss, N. Boukabcha, A. Chouaih, F. Hamzaoui, *Rasayan. J. Chem*. **2016**, *9*, 751–761.
42. M. Drissi, N. Benhalima, Y. Megrouss, R. Rahmani, A. Chouaih, F. Hamzaoui, *Molecules* **2015**, *20*, 4042–4045. **DOI:**10.3390/molecules
43. J. S. Murray, K. Sen, Molecular Electrostatic Potentials, Concepts and 399 Applications, Elsevier, Amsterdam, 1996.
44. E. Scrocco, J. Tomasi, in: P. Lowdin (Ed) Advances in Quantum Chemistry, Academic Press, New York. 1978. 402.
45. F. J. Luque, M. Orozco, P. K. Bhadane, S. R. Gadre, *J. Phys.*

Chem. **1993**, *97*, 9380–9384. **DOI:**10.1021/j100139a021
46. J. Sponer, P. Hobza, *Int. J. Quant. Chem*. **1996**, *57*, 959–970. **DOI:**10.1002/(SICI)1097-461X(1996)57:5<959::AID-QUA16>3.0.CO;2-S
47. M. Govindarajan, M. Karabacak, *Spectrochim. Acta A Mol. Biomol. Spectrosc*. **2012**, *96*, 421–435. **DOI:**10.1016/j.saa.2012.05.067

Povzetek

V prispevku poročamo o sintezi in karakterizaciji (*Z*)-3-*N*-(etil)-2-*N*'-((3-metoksifenil)imino)tiazolidin-4-ona z FT-IR, ^{1}H in ^{13}C NMR ter z rentgensko difrakcijo monokristala. Eksperimentalna potrditev kristalne strukture temelji na pridobljenih rentgenskih difrakcijskih podatkih. Pomembna značilnost strukture je obstoj dihedralnega kota, ki ga tvorita ravnini benzenskega in tiazolidinonskega obroča, v vrednosti 86.0°, kar kaže na odsotnost π–π interakcij, hkrati pa nakazuje na neplanarno strukturo. V kristalu so molekule povezane s C–H···O in C–H···N vodikovimi vezmi, ki so odgovorne za trodimenzionalno molekulsko pakiranje v strukturi. Da bi lahko eksperimentalne rezultate primerjali s teoretično izračunanimi, smo izvedli kvantno kemijske DFT izračune s pomočjo B3LYP/6-311G(d,p) baznega seta. Ob tem smo izračunali še elektrostatski potencial okoli molekule ter HOMO in LUMO energijske nivoje. Ugotovili smo orientacije dipolnih momentov in s tem razkrili naravno inter- in intramolekularnih prenosov naboja. Nazadnje smo s pomočjo izračuna deskriptorjev kemijske reaktivnosti potrdili še stabilnost opisane spojine.